

Direct visualization of phase-locking of large Josephson junction arrays by surface electromagnetic waves

M. A. Galin,^{1,2} F. Rudau,³ E. A. Borodianskyi,⁴ V. V. Kurin,¹
D. Koelle,³ R. Kleiner,³ V. M. Krasnov,^{4,2,*} and A. M. Klushin¹

¹*Institute for Physics of Microstructures RAS, 603950 Nizhny Novgorod, Russia*

²*Moscow Institute of Physics and Technology (State University), Dolgoprudny, Moscow region, 141700 Russia*

³*Physikalisches Institut and Center for Quantum Science (CQ) in LISA⁺,
Universität Tübingen, 72076 Tübingen, Germany*

⁴*Department of Physics, Stockholm University, AlbaNova University Center, SE-10691 Stockholm, Sweden*
(Dated: April 15, 2020)

Phase-locking of oscillators leads to superradiant amplification of the emission power. This is particularly important for development of THz sources, which suffer from low emission efficacy. In this work we study large Josephson junction arrays containing several thousands of Nb-based junctions. Using low-temperature scanning laser microscopy we observe that at certain bias conditions two-dimensional standing-wave patterns are formed, manifesting global synchronization of the arrays. Analysis of standing waves indicates that they are formed by surface plasmon type electromagnetic waves propagating at the electrode/substrate interface. Thus we demonstrate that surface waves provide an effective mechanism for long-range coupling and phase-locking of large junction arrays.

The creation of tunable, monochromatic, high-power and compact sources of electromagnetic (EM) waves in the 0.1-10 THz frequency range remains a serious technological challenge, colloquially known as the “THz gap” [1]. Josephson junctions (JJs) have a unique ability to generate EM radiation with tunable frequency $f = 2eV/h$, where h is the Planck constant, $2e$ is the charge of Cooper pairs and V is the dc-voltage across the JJs [2–7]. The record tunability range, 1-11 THz, [8] has been reported for intrinsic JJs in cuprate high-temperature superconductors (HTSC), for which the energy gap, determining the upper frequency limit, can be in excess of 20 THz [9, 10]. Emission power from a single JJ is small [7]. It can be amplified in the superradiant manner by phase-locking of many JJs [2–4, 11–14]. However, with an increasing number of JJs their synchronization becomes progressively more difficult due to a rapidly growing number of degrees of freedom.

Synchronization of large JJ arrays requires long-range interaction between JJs. Usually it is mediated by resonant cavity modes leading to formation of standing waves either inside [15, 16], or outside [11, 12] the JJs. With increasing array size cavity modes get damped by dissipation. For very large arrays, with sizes significantly larger than the wavelength of emitted radiation, an alternative, nonresonant mechanism of synchronization by traveling waves has been suggested and synchronization of up to 9000 JJs has been demonstrated recently [14]. Traveling waves in JJ arrays are essentially surface EM waves (SEMWs) propagating at electrode-substrate or vacuum interfaces. There is a great variety of SEMWs at metal/insulator interfaces, for a review see e.g., Ref. [17], including surface plasmons in the infrared range, which are being actively studied due to perspectives of the development of plasmonic components for optoelectronic devices [18–25]. SEMWs also exist in supercon-

ducting wires [26] and thin films [27]. Most interesting in the context of this work are leaky SEMWs [19] that facilitate emission of EM power into open space.

In this work we study Nb-based JJ arrays containing 1500 and 1660 JJs. We employ low-temperature scanning laser microscopy (LTSLM) for visualization of wave dynamics in the arrays. We observe that at certain bias voltages, corresponding to Josephson frequencies in the sub-THz range, two-dimensional standing-wave patterns appear in the arrays. Our analysis indicates that the standing waves represent interference patterns of leaky surface plasmon-type surface waves propagating in opposite directions along the electrode/substrate interface. The leakage of SEMW energy into open space facilitates both emission of EM waves and a long-range interaction between junctions in the array, which is needed for mutual phase-locking and superradiant emission.

We study arrays of serially connected Nb/Nb_xSi_{1-x}/Nb ($x \sim 0.1$) JJs. Fig. 1 shows layouts of two studied arrays, which we refer to as “linear” (a) and “meander” (b) arrays. JJs with sizes $8 \times 8 \mu\text{m}^2$ and a period of repetition of $15 \mu\text{m}$ are formed at the overlap between top and bottom Nb electrodes, as sketched in the inset. The linear array, Fig. 1(a), consists of five long parallel lines, containing 332 JJs each, thus yielding in total $N_l = 1660$ JJs. The meander array, Fig. 1(b), consists of 125 transverse strips with the length $290 \mu\text{m}$. The distance between strips is $40 \mu\text{m}$. Each strip contains 12 JJs yielding $N_m = 1500$ in total. The overall size of both arrays is 5 mm (from left to right in Fig. 1). More details about fabrication and characterization can be found in Refs. [28, 29]. Transport properties and emission characteristics of similar arrays can be found in Refs. [13, 14] and in the Supplementary [30].

We use LTSLM combined with transport measure-



FIG. 1. Geometry of studied JJ arrays. (a) Top view of the linear array. Red dots represent junctions, yellow and green stripes are Nb electrodes sequentially connecting the JJs, green rectangles at the corners are contact pads. The inset shows a schematic crosssection (side-view) of the junction area (adopted from Ref. [28]). (b) Top view of the meander array. Contact pads are outside the image area. The vertical wavy lines in (a) and (b) indicate a break in the pictures.

ments for the analysis of electric field distribution in the arrays. Previously it was demonstrated that LTSLM and a similar low-temperature scanning electron microscopy can be used for visualization of standing EM waves in JJs [31–34] and JJ arrays [35–38]. In LTSLM a focused laser beam is scanning over the sample surface causing local heating $\Delta T \lesssim 1$ K, which is small enough not to destroy superconductivity, but large enough to induce measurable changes in current-voltage characteristics (IVC's). The LTSLM image is acquired by applying a certain bias current through the array and measuring the beam-induced voltage response $\Delta U(x, y)$ upon scanning of the laser beam in the (x, y) plane. Depending on bias conditions and the temperature dependence of IVC's, ΔU can be positive or negative. $\Delta U > 0$ is due to a suppression of the critical current I_c and the switching of the junction under the beam spot from the superconducting to the resistive state. $\Delta U < 0$ is due to the reduction of the quasiparticle resistance of the junction heated by the beam. More details about LTSLM and the measurement setup can be found in the Supplementary [30].

Fig. 2(a) shows the IVC of the linear array recorded during the LTSLM measurements at the base temperature $T \simeq 6$ K. A series of current steps is seen in the IVC, as reported earlier for similar arrays [13, 14, 39]. The steps do not occur for a single JJ [29]. They are caused by wiring of JJ's in the array and, therefore, depend on electrode geometry. At lower temperature ($T \sim 4$ –5 K) it can be ascertained [30] that steps have a regular spac-

ing, $\Delta V \simeq 39$ mV, corresponding to a characteristic frequency $f_r = 2e\Delta V/hN_l \simeq 11.4$ GHz. Such a low frequency may originate only from geometrical resonances in the long, $L_l \simeq 5$ mm, straight lines of the array, see Fig. 1(a). The resonant frequency, $f_r = c/2L_l\sqrt{\epsilon^*}$, where c is the speed of light in vacuum, yields the effective dielectric permittivity $\epsilon^* \simeq 6.9$ [13, 30].

Fig. 2(b) represents LTSLM images $\Delta U(x, y)$ of a part of the linear array at four bias currents, marked by arrows in Fig. 2 (a). The horizontal scanning field, $L_x \simeq 0.91$ mm, corresponds to $\simeq 18\%$ of the total array length. At the lowest bias point A, $I = 2.0$ mA and $V \simeq 0.33$ V, some junctions (pink and blue spots) are still in the superconducting state, due to some inhomogeneity of JJs in the array. Otherwise there is no well defined spatial variation of the array response. At a slightly higher bias point B, $I = 2.17$ mA and $V \simeq 0.371$ V, a certain alternation with maxima and minima of $\Delta U(x, y)$ along the x -direction appears in the three middle lines. At point C, $I = 2.37$ mA and $V \simeq 0.409$ V, a clear standing-wave pattern develops in the whole array. It has an antisymmetric modulation with maxima in one line corresponding to minima in the neighbor lines. This is demonstrated in detail in Fig. 2(c), which represents averaged scans of $\Delta U(x)$ along each of the three middle lines of the array (blue) together with fitting curves (red). An additional minor increment of the bias current to point D, $I \simeq 2.4$ mA and $V \simeq 0.412$ V, leads to a visible reconstruction of the standing-wave pattern. Here it becomes almost symmetric with aligned maxima and minima in all the lines.

The increase of voltage leads to the growth of the Josephson frequency and a reduction of the wavelength of EM radiation. Indeed, such a tendency can be traced from Fig. 2(b). The Josephson frequencies at points B, C and D are: $f(B) \simeq 107.8$ GHz, $f(C) \simeq 119.0$ GHz and $f(D) \simeq 119.9$ GHz. The corresponding periods of standing waves are $\Delta x(B) = 0.53$ mm, $\Delta x(C) = 0.47$ mm, and $\Delta x(D) = 0.46$ mm. Since LTSLM probes only the EM amplitude, the EM wavelength is twice the period of LTSLM image, $\lambda = 2\Delta x$. The observed decrease of λ with increasing f follows a simple relation $\lambda = c/f\sqrt{\epsilon^*}$ with $\epsilon^* = 6.9 \pm 0.2$, consistent with the estimation above from the step voltages in the IVC.

The observation of a correlated two-dimensional standing-wave order indicates a global synchronization of the whole array. We did LTSLM scans over a broad bias range along the IVC. However, such correlated standing wave patterns were observed only in a limited bias range from slightly below the point B to slightly above the point D. This is qualitatively consistent with a narrow bias range in which significant EM wave emission occurs from such an array [30].

Fig. 3(a) shows the IVC of the meander array recorded during LTSLM measurements at $T \simeq 5$ K. Similar to the linear array, the IVC of the meander array also has dis-

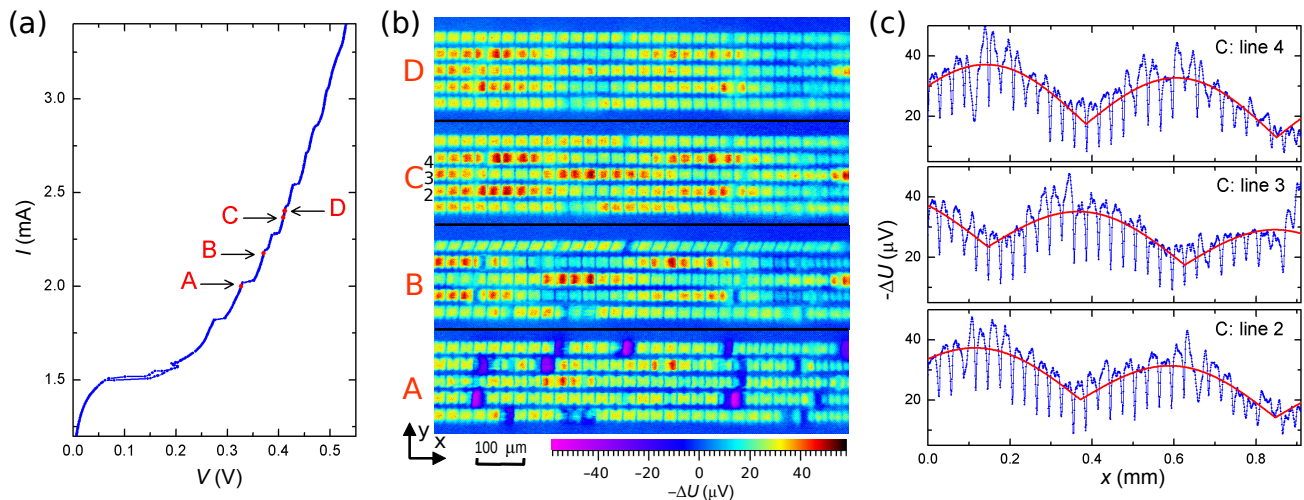


FIG. 2. LTSLM analysis of the linear JJ array at $T \sim 6$ K. (a) I - V characteristic of the array measured during LTSLM imaging. (b) LTSLM images obtained at four bias points, indicated in (a). The length of scans along x -axis is $L_x = 0.91$ mm. The scans are stretched about 2 times along y -axis for better viewing. Development of standing-wave correlations is clearly seen in patterns B, C and D. (c) LTSLM response (blue lines) along horizontal array lines 2–4 (from bottom to top as indicated in (b), panel C) for the pattern C, $I = 2.37$ mA. The data are averaged over the width of strip. Red lines represent fitting curves obtained by the method of least squares. Antisymmetric modulation in neighbor lines is seen.

tinct resonant steps. Fig. 3(b) represents LTSLM images of the meander array at different bias points marked in Fig. 3(a). A: $I = 1.86$ mA and $V = 144$ mV, B: $I = 1.9$ mA and $V = 174$ mV, C: $I = 1.95$ mA and $V = 200$ mV, D: $I = 2.18$ mA and $V \simeq 263$ mV. Note that the IVC of the meander array exhibits a hysteresis, presumably due to self-heating. Points A–C are measured at the reverse part of the IVC within the hysteretic area. LTSLM images are taken at the right end of the array with the same field of view as in Fig. 2 (b), $L_x \simeq 0.91$ mm, which encompasses 22 transverse strips.

Standing wave patterns in the horizontal direction can be seen in all images of Fig. 3 (b). The periodicity Δx is gradually decreasing with increasing voltage from A to D: in A it is about five transverse strips and in D about three. This is in a qualitative agreement with the expected decrease of the wavelength with increasing frequency. However, if we calculate the speed of EM wave propagation along the x -axis, $c_x = 2\Delta x f$, with $f = 2eV/hN_m$, we obtain unreasonably low values. For example, at bias point A the periodicity along the horizontal axis is $\Delta x \simeq 200 \mu\text{m}$, which yields $c_x \simeq 1.8 \times 10^7$ m/s $\simeq 0.06c$. This would require a huge dielectric constant $\varepsilon^* \sim 300$, which does not make sense. Therefore, the observed standing-waves in the meander array can not be caused by propagation of a volume EM wave in some media. This conclusion is also confirmed by the observation that with changing frequency the nodal areas (blue color) are shifting along the meander line and may start/end at an arbitrary place of the transverse strips. E.g. in A they usually start/end at the edges, but in C

- in the middle of the strips. Thus, the standing wave pattern is not periodic along the horizontal x -axis, as would be expected for a straightforward EM-wave propagation in the substrate. Those inconsistencies, revealed by a specific meander geometry of the array, which has a large geometrical deceleration [40], provide a clue to understanding of the nature of EM waves in our arrays.

In Fig. 3(c) we plot the LTSLM response for the image C (top) and D (bottom panel) along the meander line, as a function of the overall length of the Nb electrode from the bottom-left to the bottom-right edges of the images in the Fig. 3b. From this plot it becomes clear that there is a long-range standing wave order *along the electrode*. The periodicity is $\Delta l = 1.23$ mm for the image C and $\Delta l = 0.85$ mm for the image D. The corresponding phase velocities, $c^* = 2\Delta l f$, are C: $\simeq 1.59 \times 10^8$ m/s and D: $\simeq 1.44 \times 10^8$ m/s, which yield a reasonable $\varepsilon^* \simeq 4.0 \pm 0.3$ [41]. The performed estimations unambiguously prove that EM waves, building the standing wave, are propagating along the electrode line and a significant value of ε^* indicates that they propagate at the Nb/substrate side. This is a signature of surface EM waves at metal/insulator interfaces [17–27].

Another confirmation of SEMW character of standing wave resonances in the meander array comes from transport measurements. At low temperatures we observe a very fine step structure in the IVC (see the Supplementary [30]) with a typical voltage separation $\Delta V \simeq 7$ mV. It yields a very low primary resonant frequency $f_r \simeq 2.3$ GHz corresponding to a long resonator length $\simeq 3$ cm, which is consistent with the total length

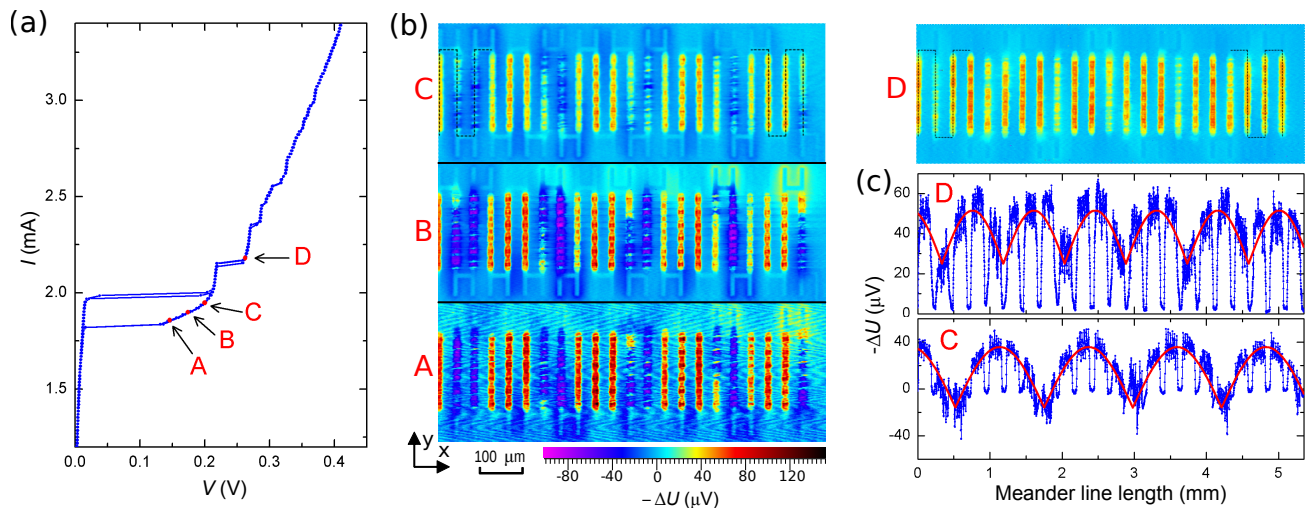


FIG. 3. LTSLM analysis of the meander array at $T \sim 5$ K. (a) I - V characteristic of the array, measured during LTSLM imaging. (b) LTSLM images at different bias points, indicated in (a). The length of scans along x -axis is $L_x = 0.91$ mm. Development of standing-wave pattern is clearly seen. Note that the standing wave is not periodic in the horizontal direction. Dot lines indicate the start and the end of track along the length of the meander line where the periodicity of response is observed. (c) LTSLM responses (blue lines) along the tracks indicated in (b) from the bottom-left to the bottom-right corner of the pattern at the bias points C (top) and D (bottom). The data are averaged over the width of strip. Red line represents fitting curves obtained by the method of least squares. Clear periodicity along the whole meander length indicates that standing waves are formed by plasmon-type surface waves propagating along Nb electrodes.

of the meandering line. This confirms that such resonances are formed by traveling surface waves bound to Nb electrodes.

There are many known modes of SEMWs [17]. While we can not provide a decisive distinction of the SEMW mode in our case, we argue that the intermediate value of $\varepsilon^* \sim 6.9 - 4.0$ inbetween Si (11.9) and vacuum (1) suggests that those are leaky surface-plasmon-type SEMWs propagating along one interface and leaking energy at the opposite interface of the metallic film [19]. However, the actual sub-THz frequency is well below the plasma frequency. Consequently they correspond to the linear part of the dispersion relation for surface plasmons (for an additional discussion see the Supplementary [30]). Importantly, the leaky nature of the involved SEMW both facilitates long-range synchronization of a large array and enables EM wave emission into open space. All this is a prerequisite for creation of a high-power coherent THz oscillator.

To conclude, synchronization of large oscillator arrays is a challenging problem. In this work we performed simultaneous transport measurements and low-temperature scanning laser microscopy of large arrays with 1500 and 1660 Josephson junctions. Our main result was the observation of standing-wave patterns, indicating global phase-locking of the arrays. From an analysis of the evolution of standing wave patterns with changing Josephson frequency we deduced that those patterns are formed by plasmon-type surface EM waves propa-

gating along electrodes at the superconductor/substrate interface. We conclude that such type of surface waves can facilitate both emission of power and phase-locking of very large oscillator arrays, which is required for creation of high-power THz sources.

ACKNOWLEDGEMENTS

We are grateful to F. Müller and Th. Scheller (PTB Braunschweig, Germany) for sample fabrication. V.M.K. is grateful for hospitality during a sabbatical period at MIPT, arranged via the 5-top-100 program. The work was supported by the Russian Science Foundation, grant No. 20-42-04415 (experimental part: carrying out the measurements - Figs. 2(a), 2(b), 3(a), 3(b)), the Russian Foundation for Basic Research, grant No. 18-02-00912 (theoretical part: fitting - Figs. 2(c), 3(c)), the State Contract No. 0035-2019-0021 "Transport properties and electrodynamics of nanostructural superconductors and hybrid systems: quantum effects and nonequilibrium states", the Deutsche Forschungsgemeinschaft via project KL930/17-1, the COST action NANOCOHBRI (CA16218), European Union H2020-WIDESPREAD-05-2017-Twinning project SPINTECH under Grant Agreement No. 810144 and the Swedish Research Council, project 2018-04848.

- * vladimir.krasnov@fysik.su.se
- [1] M. Tonouchi, Cutting-edge terahertz technology. *Nature Photonics* **1**, 97 (2007).
 - [2] U. Welp, K. Kadowaki, and R. Kleiner, Superconducting emitters of THz radiation, *Nature Photonics* **7**, 702 (2013).
 - [3] L. Ozyuzer, A. E. Koshelev, C. Kurter, N. Gopalsami, Q. Li, M. Tachiki, K. Kadowaki, T. Yamamoto, H. Minami, H. Yamaguchi, T. Tachiki, K. E. Gray, W.-K. Kwok, and U. Welp, Emission of Coherent THz Radiation from Superconductors, *Science* **318**, 1291 (2007).
 - [4] T.M. Benseman, K. E. Gray, A. E. Koshelev, W.-K. Kwok, U. Welp, H. Minami, K. Kadowaki, and T. Yamamoto, Powerful terahertz emission from $\text{Bi}_2\text{Sr}_2\text{CaCu}_2\text{O}_{8+\delta}$ mesa arrays. *Appl. Phys. Lett.* **103**, 022602 (2013).
 - [5] M. Ji, J. Yuan, B. Gross, F. Rudau, D. Y. An, M. Y. Li, X. J. Zhou, Y. Huang, H. C. Sun, Q. Zhu, J. Li, N. Kinev, T. Hatano, V. P. Koshelets, D. Koelle, R. Kleiner, W. W. Xu, B. B. Jin, H. B. Wang, and P. H. Wu, $\text{Bi}_2\text{Sr}_2\text{CaCu}_2\text{O}_8$ intrinsic Josephson junction stacks with improved cooling: Coherent emission above 1 THz. *Appl. Phys. Lett.* **105**, 122602 (2014).
 - [6] T. Kashiwagi, T. Yamamoto, T. Kitamura, K. Asanuma, C. Watanabe, K. Nakade, T. Yasui, Y. Saiwai, Y. Shibano, H. Kubo, K. Sakamoto, T. Katsuragawa, M. Tsujimoto, K. Delfanazari, R. Yoshizaki, H. Minami, R. A. Klemm, and K. Kadowaki, Generation of electromagnetic waves from 0.3 to 1.6 terahertz with a high- T_c superconducting $\text{Bi}_2\text{Sr}_2\text{CaCu}_2\text{O}_{8+\delta}$ intrinsic Josephson junction emitter, *Appl. Phys. Lett.* **106**, 092601 (2015).
 - [7] V.P. Koshelets and S.V. Shitov, Integrated superconducting receivers, *Supercond. Sci. Technol.* **13**, R53 (2000).
 - [8] E. A. Borodianskyi and V.M. Krasnov, Josephson emission with frequency span 1–11 THz from small $\text{Bi}_2\text{Sr}_2\text{CaCu}_2\text{O}_{8+\delta}$ mesa structures, *Nat. Commun.* **8**, 1742 (2017).
 - [9] S.O. Katterwe, H. Motzkau, A. Rydh, and V.M. Krasnov, Coherent generation of phonon-polaritons in $\text{Bi}_2\text{Sr}_2\text{CaCu}_2\text{O}_{8+x}$ intrinsic Josephson junctions, *Phys. Rev. B* **83**, 100510(R) (2011).
 - [10] V.M. Krasnov, Interlayer tunneling spectroscopy of $\text{Bi}_2\text{Sr}_2\text{CaCu}_2\text{O}_{8+d}$: A look from inside on the doping phase diagram of high- T_c superconductors *Phys. Rev. B* **65**, 140504(R) (2002).
 - [11] P. Barbara, A.B. Cawthorne, S.V. Shitov, and C. J. Lobb, Stimulated Emission and Amplification in Josephson Junction Arrays, *Phys. Rev. Lett.* **82**, 1963 (1999).
 - [12] F. Song, F. Müller, R. Behr, and A.M. Klushin, Coherent emission from large arrays of discrete Josephson junctions, *Appl. Phys. Lett.* **95**, 172501 (2009).
 - [13] M. A. Galin, A.M. Klushin, V. V. Kurin, S. V. Seliverstov, M. I. Finkel, G. N. Goltsman, F. Müller, T. Scheller, and A.D. Semenov, Towards local oscillators based on arrays of niobium Josephson junctions, *Supercond. Sci. Technol.* **28**, 055002 (2015).
 - [14] M. A. Galin, E. A. Borodianskyi, V. V. Kurin, I. A. Shereshevskiy, N.K. Vdovicheva, V.M. Krasnov, and A.M. Klushin, Synchronization of Large Josephson-Junction Arrays by Traveling Electromagnetic Waves, *Phys. Rev. Appl.* **9**, 054032 (2018).
 - [15] V. M. Krasnov, Coherent flux-flow emission from stacked Josephson junctions: Nonlocal radiative boundary conditions and the role of geometrical resonances. *Phys. Rev. B* **82**, 134524 (2010).
 - [16] V. M. Krasnov, Terahertz electromagnetic radiation from intrinsic Josephson junctions at zero magnetic field via breather-type self-oscillations. *Phys. Rev. B* **83**, 174517 (2011).
 - [17] T.K. Sarkar, M.N. Abdallah, M. Salazar-Palma, and W.M. Dyab, Surface Plasmons/ Polaritons, Surface Waves, and Zenneck Waves: Clarification of the terms and a description of the concepts and their evolution. *IEEE Antennas & Propagation Magazine* **59**, 78-93 (2017). DOI:10.1109/MAP.2017.2686079
 - [18] E. N. Economou, Surface Plasmons in Thin Films. *Phys. Rev.* **182**, 539 (1969).
 - [19] J. J. Burke, G. I. Stegeman, and T. Tamir, Surface-polariton-like waves guided by thin, lossy metal films. *Phys. Rev. B* **33**, 5186 (1986).
 - [20] E. Ozbay, Plasmonics: Merging Photonics and Electronics at Nanoscale Dimensions. *Science* **311**, 189 (2006).
 - [21] R. W. Heeres, S. N. Dorenbos, B. Koene, G. S. Solomon, L. P. Kouwenhoven, and V. Zwiller, On-Chip Single Plasmon Detection. *Nano Lett.* **10**, 661 (2010).
 - [22] M. Kauranen and A.V. Zayats, Nonlinear plasmonics, *Nature Photonics* **6**, 737 (2012).
 - [23] Z. Zalevsky and I. Abdulhalim, Integrated Nanophotonic Devices, Second Edition (2014 Elsevier Inc.), ISBN: 978-0-323-22862-6. DOI:10.1016/B978-0-323-22862-6.00006-2.
 - [24] M.I. Stockman, et al., Roadmap on plasmonics, *J. Opt.* **20**, 043001 (2018).
 - [25] L. Yin, V. K. Vlasko-Vlasov, J. Pearson, J. M. Hiller, J. Hua, U. Welp, D. E. Brown, and C. W. Kimball, Sub-wavelength Focusing and Guiding of Surface Plasmons. *Nano Lett.* **5**, 1339 (2005).
 - [26] B. Camarota, F. Parage, F. Balestro, P. Delsing, and O. Buisson, Experimental Evidence of One-Dimensional Plasma Modes in Superconducting Thin Wires. *Phys. Rev. Lett.* **86**, 480 (2001).
 - [27] K.L. Ngai, Interaction of ac Josephson Currents with Surface Plasmons in Thin Superconducting Films. *Phys. Rev.* **182**, 555 (1969).
 - [28] F. Mueller, R. Behr, T. Weimann, L. Palafox, D. Olaya, P. D. Dresselhaus, and S. P. Benz, 1 V and 10 V SNS Programmable Voltage Standards for 70 GHz, *IEEE Trans. Appl. Supercond.* **19**, 981 (2009).
 - [29] D. Olaya, P.D. Dresselhaus, S.P. Benz, A. Herr, Q.P. Herr, A.G. Ioannidis, D.L. Miller and A. W. Kleinsasser, Digital circuits using self-shunted Nb/Nb_xSi_{1-x}/Nb Josephson junctions, *Appl. Phys. Lett.* **96**, 213510 (2010).
 - [30] See supplementary material at ... which contains clarifications about LTSLM technique, complementary transport and radiation measurements and an additional discussion about surface electromagnetic waves.
 - [31] B. Mayer, T. Doderer, R. P. Huebener, and A. V. Ustinov, Imaging of one- and two-dimensional Fiske modes in Josephson tunnel junctions, *Phys. Rev. B* **44**, 12463 (1991).
 - [32] C. A. Kruelle, T. Doderer, D. Quenter, R. R. Huebener, R. Pöpel, and J. Niemeyer, Standing wave patterns of microwaves propagating in Josephson tunnel junctions with integrable and chaotic billiard geometries, *Physica D* **78**,

- 214 (1994).
- [33] D. Quenter, A. V. Ustinov, S. G. Lachenmann, T. Doderer, R. P. Huebener, F. Müller, J. Niemeyer, R. Pöpel, and T. Weimann, Spatially resolved flux flow in long-overlap Josephson tunnel junctions, *Phys. Rev. B* **51**, 6542 (1995).
- [34] R. Gerber, D. Quenter, T. Doderer, C. A. Kruelle, R. P. Huebener, F. Müller, J. Niemeyer, R. Pöpel, and T. Weimann, Quantitative measurement of the microwave distribution in superconducting tunnel junctions, *Appl. Phys. Lett.* **66**, 1554 (1995).
- [35] H. B. Wang, S. Guenon, J. Yuan, A. Iishi, S. Arisawa, T. Hatano, T. Yamashita, D. Koelle, and R. Kleiner, Hot Spots and Waves in $\text{Bi}_2\text{Sr}_2\text{CaCu}_2\text{O}_8$ Intrinsic Josephson Junction Stacks: A Study by Low Temperature Scanning Laser Microscopy, *Phys. Rev. Lett.* **102**, 017006 (2009).
- [36] A. Laub, M. Keck, T. Doderer, R. P. Huebener, T. Traeuble, R. Dolata, T. Weimann, and J. Niemeyer, The influence of the critical current spread on the frequency locking of Josephson junctions in two-dimensional arrays, *J. Appl. Phys.* **83**, 5302 (1998).
- [37] M. Keck, T. Doderer, R. P. Huebener, T. Traeuble, R. Dolata, T. Weimann, and J. Niemeyer, Spatially resolved detection of phase locking in Josephson junction arrays, *Applied Superconductivity* **6**, 297 (1998).
- [38] S. G. Lachenmann, T. Doderer, D. Hoffmann, R. P. Huebener, P. A. A. Booij and S. P. Benz, Observation of vortex dynamics in two-dimensional Josephson-junction arrays, *Phys. Rev. B* **50**, 3158 (1994).
- [39] F. Song, F. Müller, T. Scheller, A. Semenov, M. He, L. Fang, H. W. Hübers, and A. M. Klushin, Compact tunable sub-terahertz oscillators based on Josephson junctions, *Appl. Phys. Lett.* **98**, 142506 (2011).
- [40] D. A. Gandolfo, A. Boornard, and L. C. Morris, Superconductive Microwave Meander Lines, *J. Appl. Phys.* **39**, 2657 (1968).
- [41] For the meander array ε^* is smaller by a factor $\sim 1.6-1.9$ than for the linear array. This may be due to a known effect of reduction of the effective length of bent antennas, see e.g. D. M. Dobkin, in *The RF in RFID: passive UHF RFID in practice*, 1st ed. (Newnes, USA, 2008), Chap. 7. It may lead to the reduction of the actual SEMW propagation length (shortcutting) at the turns of the meander line and, thus, to an overestimation of the wavelength and underestimation of ε^* . For the meander array there is also some variation of the estimated ε^* between points A-C, which might be caused by a not well known number of active junctions within the hysteresis part of the IVC, which would affect the estimation of the Josephson frequency.